Guinier pattern of the binary phase but not for Zr_5Si_3O, either for the arc melted or the better sintered sample. Obviously, the same general condition applies to carbon; a faint (100) reflection was seen for $Zr_5Si_3C_{0.33}$ but not for the carbon-richer samples.

Although not tested, we presume that at least boron and nitrogen can be bound in Zr_5Si_3 and will produce similar dimensional effects, boron the most positive. The analogous Zr_5Sn_3 and Zr_5Sb_3 form stoichiometric ternary phases with C, N, O, Al, Si, etc., and in these only second-period elements cause marked contractions of the cells. Fractional occupancy in ordered superstructures as found for $La_{15}Ge_9C$ has not been observed in zirconium systems.

Comparison of our lattice constant data with earlier reports for supposed Zr_5Si_3 (Table II) suggests that most were seriously contaminated, probably by the more pervasive nonmetals. Some dimensions and volumes fall well below what we have been able to achieve with oxygen alone, even in earlier studies that utilized iodide–zirconium. The only exception is a 1964 study of a single crystal isolated at ~2200 °C from molten alloy $Zr_5Si_{3.56}$ that had been prepared from 99.6% Zr and 99.7% Si.[24] A simple-minded interpretation of the dimensions suggests 30–50% of the oxygen limit Zr_5Si_3O. Of course, the sample may have been nonstoichiometric at that temperature or contaminated by third-period and heavier elements that would mask a dimensional view of the true situation.

These investigations of La_5Sn_3 and Zr_5Si_3 highlight the problems that impurities can have on stability of supposed binary phases. Our studies have focused particularly on those examples in the rather common Mn_5Si_3 structure where an avidity for binding impurity atoms interstitially within confacial manganese octahedra seems particularly strong. Phases of this general character have been designated "Nowotny phases" after the early investigator of many examples in this and other structure types.[14] Many other unrecognized examples of such effects or errors are presumably present in the literature. Oxygen is a particularly common and troublesome example with lanthanum, zirconium, and related metals.

Acknowledgment. We are especially indebted to H. F. Franzen for the use of the arc-melting and induction furnaces and to V. I. Tsirelnikov for a copy of ref 31. M.A.R. supported by the NSF-sponsored Summer Research Program in Solid State Chemistry (DMR).

Registry No. La_5Sn_3, 12209-13-1; $La_5Sn_3C_{0.5}$, 129124-12-5; $La_5Sn_3C_{0.75}$, 129124-13-6; La_5Sn_3C, 129124-14-7; $La_5Sn_3C_2$, 129124-15-8; $La_5Sn_3O_{0.3}$, 129124-16-9; La_5Sn_3O, 129124-17-0; Zr_5Si_3, 12039-97-3; $Zr_5Si_{2.8}$, 129124-18-1; $Zr_5Si_{3.1}$, 129124-19-2; $Zr_5Si_3C_{0.5}$, 129124-20-5; Zr_5Si_3C, 129124-21-6; Zr_5Si_3O, 129124-22-7; $Zr_5Si_{3.56}$, 129124-23-8.

Substituted W_5Si_3- and Zr_6Al_2Co-Type Phases Formed in the Zirconium–Antimony and Zirconium–Tin Systems with Iron Group Metals

Young-Uk Kwon, Slavi C. Sevov, and John D. Corbett*

Department of Chemistry and Ames Laboratory—DOE,[1] Iowa State University, Ames, Iowa 50011

Received June 4, 1990

Arc-melting and annealing reactions near the composition Zr_5Sb_3Fe yield $ZrFe_2$ plus an Mn_5Si_3-type phase with a composition near $Zr_5Sb_{3.3}Fe_{0.3}$. A lower antimony content and a variety of iron group metals produce tetragonal W_5Si_3-type phases with a narrow compositional range, $\sim Zr_5Sb_{2.5}T_{0.5}$, T = Fe, Co, Ni, Ru, Rh. A single-crystal study of the W_5Si_3-type $Zr_5Sb_{2.55(1)}Fe_{0.45(1)}$ established a mixed Sb–Fe population on the Sb1 site centering the Zr2 antiprisms ($I4/mcm$, $Z = 4$, $a = 11.066$ (1) Å, $c = 5.535$ (1) Å, $R/R_w = 1.9/2.8\%$). The analogous Zr–Sn–Fe system contains a W_5Si_3-like phase $Zr_5Sn_{2+x}Fe_{1-x}$, $0 \leq x \leq 0.28$, but in this case with a lower symmetry tetragonal cell that has distinctly different mixed Fe–Sn populations centering adjacent Zr2 antiprisms (91 (2) and 52 (2)% Fe for $x = 0.28$) ($I422$, $Z = 4$, $a = 11.1763$ (7) Å, $c = 5.4794$ (6) Å, $R/R_w = 1.7/2.2\%$). The lower symmetry cannot be deduced from powder pattern data. The hexagonal line phase Zr_6Sn_2Fe, previously known as the θ phase, is obtained when still more zirconium is present (Zr_6Al_2Co structure, $P\bar{6}2m$, $Z = 1$, $a = 7.9675$ (6) Å, $c = 3.4863$ (5) Å, $R/R_w = 2.6/2.9\%$). Antimony systems provide analogous substitutional products $\sim Zr_5Sb_{2.3}T_{0.7}$, T = Fe, Co, Ni. Some regularities associated with the three structure types are discussed.

Introduction

Our intensive studies of Zr_5Sb_3–Zr_5Sb_3Z and Zr_5Sn_3–Zr_5Sn_3Z systems have shown that phases with the parent Mn_5Si_3-type structure exist for a wide range of Z as an interstitial component.[2-4] However, attempts to introduce iron in this position in either system have been troublesome. These have always led to $ZrFe_2$ precipitation and to a phase with the Mn_5Si_3 structure but with evidently mixed Sb–Fe or Sn–Fe interstitials judging from SEM analyses.[2,4,5] Attempts to avoid the mixed products by decreasing the amount of antimony or tin produced new tetragonal phases. We herein report the identification of these as W_5Si_3-type structures or a lower symmetry version of the same in which iron has been systematically substituted for some of the Sb or Sn atoms. The stabilization

(1) The Ames Laboratory—DOE is operated for the U.S. Department of Energy by Iowa State University under Contract No. W-7405-Eng-82. This research was supported by the Office of Basic Energy Sciences, Materials Sciences Division.

(2) Garcia, E.; Corbett, J. D. *Inorg. Chem.* **1988**, *27*, 2907; **1990**, *29*, 3274.

(3) Corbett, J. D.; Garcia, E.; Kwon, Y.-U.; Guloy, A. *Pure Appl. Chem.* **1990**, *62*, 103.

(4) Kwon, Y.-U.; Corbett, J. D., unpublished research.

(5) Sevov, S. C.; Corbett, J. D., unpublished research.

of these phases by iron has also been explored for the neighboring transition metals (T) Co and, in part, Ni, Ru, and Rh. We also attempted to repress the formation of mixed products by the addition of more zirconium. This led instead to the formation of hexagonal phases, Zr_6Sn_2Fe, for example, with the Zr_6Al_2Co structure.

Experimental Section

Materials. The zirconium metal was a reactor-grade crystal bar sample with principal impurities, in ppm atomic, of Fe 680, Ni 350, Hf 100, O 220, and C 190. This was cold-rolled to sheet, cut into strips, and cleaned with a solution of concentrated HNO_3 and HF in H_2O (55:25:20 v/v). The reagent-grade antimony (Allied Chemical and Dye Co.) showed no impurities in its EDX spectra, and the tin granules (Baker's Analyzed: 99.99%) produced no impurity phases on fusion. Iron sheet (Plastic Metal, 99.5%), cobalt foil (Aesar, 99.9+%), nickel sheet (Matheson Coleman & Bell), rhodium powder (Aesar, 99.9%), and ruthenium powder (Englhard, 99.9%) were used as received.

Syntheses. All the samples were first prepared by arc-melting reactions, as before.[2,6] For rhodium and ruthenium compounds, the metal powders were first pelletized with zirconium and arc-melted to give the compositions of Zr_5Rh_2 and Zr_5Ru_2, and these were used as reagents for further reactions. Stoichiometric proportions of the elements or binary compounds were arc-melted in a Centorr 5SA single arc-furnace under an argon atmosphere. In each case, zirconium was first melted as a getter. Product buttons were turned over and remelted at least three times to ensure homogeneity. The compositions of samples so prepared were corrected by assuming that the small weight losses during melting arose solely from tin or antimony volatilization.

Since arc-melting alone may produce heterogeneous or somewhat disordered products, the buttons were next annealed in sealed Ta containers containing 0.08-mm Mo sheet as liners. The latter were found to be indispensable because sample contact with tantalum alone may lead to a significant loss of zirconium above ~1000 °C.[4,5] This observation was well exemplified by an annealing reaction of a composition Zr_5Sn_2Fe which converted into Zr_5Sn_3 and $ZrFe_2$ when contained in tantalum alone (1000 °C, 9 days), while equilibration of the sample in contact with only Mo at 1350 °C produced the desired phase. The tantalum containers were in turn always enclosed in evacuated and sealed silica jackets for annealing reactions at 1100 °C or below. At higher temperatures, these were equilibrated under dynamic vacuum ($p \sim 10^{-6}$ Torr) in a high-temperature carbon furnace described elsewhere.[7] Container or other impurity elements were not detectable by SEM-EDX means in any of the products.

SEM Studies. Photomicrographs and elemental analyses of the samples were obtained by using a JEOL JSM-840 scanning electron microscope and a KEVEX EDX system. Samples were dry-polished with a sequence of very fine sandpapers and then ash. Quoted formulas are probably uncertain in the atom coefficients by about ±0.05.

Powder X-ray Diffraction. Powder patterns were obtained on samples mounted between pieces of cellophane tape. An Enraf-Nonius Guinier camera, Cu Kα radiation (λ = 1.540 56 Å), and NBS (NIST) silicon as an internal standard were employed for this purpose. The known 2θ values of the standard lines were fitted to a quadratic in their positions on the film, and the lattice constants of the sample then calculated by a least-squares fit to indexed reflections and their 2θ values.

The powder pattern of the so-called θ-phase (Zr_6Sn_2Fe) was indexed as hexagonal by trial-and-error means.[8] The volume of the unit cell and the approximate composition allowed an estimation of nine atoms per unit cell. Only one known structure type, Zr_6Al_2Co,[9] was found to match this formulation and symmetry,[10] and the powder pattern calculated by using the positional parameters of the parent structure and the refined lattice parameters matched the observed one reasonably well. The single crystal structural analysis (below) subsequently confirmed the assignment.

Table I. Selected Data Collection and Refinement Parameters

	$Zr_5Sb_{2.55}Fe_{0.45}$	$Zr_5Sn_{2.3}Fe_{0.7}$	Zr_6Sn_2Fe
space group, Z	*I*4/*mcm*, 4	*I*422, 4	$P\bar{6}2m$, 1
cell dimensions[a]			
a, Å	11.066 (1)	11.1763 (7)	7.9675 (6)
c, Å	5.535 (1)	5.4794 (6)	3.4863 (5)
V, Å^3	667.8 (2)	684.4 (1)	191.66 (4)
2θ(max)	75	55	60
indep reflns	376	350	196
μ(Mo Kα), cm^{-1}	180.3	164.4	159.6
transm factor range	0.77–1.00	0.75–1.00	0.71–1.00
R,[b] %	1.9	1.7	2.6
R_w,[b] %	2.8	2.2	2.9

[a] Cell data from Guinier powder diffraction, λ = 1.540 56 Å. [b] $R = \sum||F_o| - |F_c||/\sum|F_o|$; $R_w = [\sum w(|F_o| - |F_c|)^2/\sum w(F_o)^2]^{1/2}$; $w = [\sigma(F_o)]^{-2}$.

Single-Crystal Analyses. Three crystal structures were refined with the aid of the TEXSAN package[11] and diffraction data from single crystals that were collected at room temperature on a Rigaku AFC6R single-crystal diffractometer with monochromated Mo Kα radiation. Reflections in two octants were measured with 2θ–ω scans in all cases. Some details of the data collection and refinement are listed in Table I. Unique aspects of the crystallography follow:

$Zr_5Sb_{2.5}Fe_{0.5}$. Single crystals resembling cut gems were picked from an as-cast sample of nominal composition $Zr_5Sb_{2.55}Fe_{0.67}$ that exhibited only trace amounts of other phases (see Results); the crystals were loaded in air into thin-walled glass capillaries and sealed off. The candidate crystals were checked with oscillation photographs, and one of them (no clear morphology, 0.5 × 0.5 × 0.4 mm) was selected for data collection. The 25 reflections found from a random search were indexed with a body-centered tetragonal cell. The body centering was also indicated by its previously indexed powder pattern, and therefore this condition was imposed for data collection. After correction for absorption with the aid of a ψ-scan, the diffraction data showed additional systematic absences of $0kl$ ($k,l \neq 2n$) with two very weak violations. Among the three possible space groups, *I*4*cm*, $I\bar{4}2m$ and *I*4/*mcm*, the last, centrosymmetric one was chosen for the first trial, and this turned out to be correct.

The application of direct methods (SHELXS-86[12]) gave two positions, and these were assigned as Sb2 and Zr1 for the starting model. One cycle of least-squares refinement and a difference Fourier synthesis revealed two more atoms, Zr2 and Fe. Refinement with isotropic thermal parameters proceeded smoothly (R = 9%), but this resulted in an unreasonably small thermal parameter for Fe. The next step was to include antimony (Sb1) in the iron position with the condition that the Sb1 and Fe occupancies sum to unity. The final refinement converged at R = 1.9%, R_w = 2.8% with the refined formula $Zr_5Sb_{2.55(1)}Fe_{0.45(1)}$, in excellent accord with the EDX result as well as close to the loaded composition. The multiplicities of Zr2 and Sb2 did not deviate from unity by more than 0.5% with Zr1 fixed, and therefore these were not varied in the final refinement. The largest residual peaks in the final difference Fourier, 2.3 and −2.0 e/Å^3 were <1 Å from Zr2. The result was later recognized as a substituted W_5Si_3-type structure.

$Zr_5Sn_{2.3}Fe_{0.7}$. Some single crystals were picked from a crushed button of the composition Zr_5Sn_2Fe that had been annealed at 1350 °C (see Results). The powder pattern could be entirely accounted for by a tetragonal W_5Si_3-type phase plus a small amount of $ZrFe_2$. The crystals were checked with oscillation

(6) Kwon, Y.-U.; Corbett, J. D. *Chem. Mater.* **1990**, *2*, 27.
(7) Kwon, Y.-U.; Rzeznik, M. A.; Guloy, A.; Corbett, J. D. *Chem. Mater.*, previous article in this issue.
(8) Werner, P. E. TREOR-4. Trial and Error Program for Indexing of Unknown Powder Patterns...; Department of Structural Chemistry, Arrhenius Laboratory, University of Stockholm, Sweden, 1984.
(9) Krypyakevich, P. I.; Burnashova, V. V.; Markiv, V. Ya. *Dopov. Akad. Nauk. Ukr. RSR, Ser. A: Fiz-Tekhn. Mat. Nauki* **1970**, *32*, 828.
(10) Villars, P.; Calvert, L. D. *Pearson's Handbook of Crystallographic Data for Intermetallic Phases*; America Society of Metals: Metals Park, OH, 1985; Vol. 1, pp 506, 559, 580.
(11) TEXSAN, Version 5.0, Molecular Structure Corp., The Woodlands, TX, 1989.
(12) Sheldrick, G. M. Universität Göttingen, FRG, 1986.

Table II. Positional Parameters and Multiplicities of Atoms

atoms	occup[a]	sym	x	y	z	B_{iso}, Å^2
			$Zr_5Sb_{2.55}Fe_{0.45}$ (W_5Si_3-Type)			
Zr1	1	*m*	0	$^1/_2$	$^1/_4$	0.47 (2)
Zr2	1	$\bar{4}2m$	0.076 75 (4)	0.215 93 (5)	0	0.51 (2)
Sb2	1	*mm*	0.163 02 (3)	$x + ^1/_2$	0	0.47 (1)
Sb1	0.55 (1)	42	0	0	$^1/_4$	0.72 (2)
Fe	0.45 (1)					
			$Zr_5Sn_{2.3}Fe_{0.7}$ (W_5Si_3 Derivative)			
Zr1	1.000 (4)	222	0	$^1/_2$	0	0.6 (1)
Zr2	1	1	0.075 52 (4)	0.210 43 (4)	0.7482 (4)	0.79 (2)
Sn2[b]	1.009 (3)	2	0.163 75 (3)	$x + ^1/_2$	$^3/_4$	0.57 (1)
Sn1	0.09 (2)	42	0	0	0	0.7 (2)
Fe1	0.91 (2)					
Sn3	0.48 (2)	42	0	0	$^1/_2$	0.8 (1)
Fe2	0.52 (2)					
			Zr_6Sn_2Fe (Zr_6Al_2Co-Type)			
Zr1	1	*mm*	0.3929 (2)	0	0	0.63 (6)
Zr2	0.996 (8)	*mm*	0.7548 (1)	0	$^1/_2$	0.50 (5)
Sn	0.990 (6)	$\bar{6}$	$^1/_3$	$^2/_3$	$^1/_2$	0.64 (2)
Fe	1.00 (1)	$\bar{6}m2$	0	0	0	0.75 (6)

[a] The mixed-atom populations and the compounds' crystal compositions are based on the assumption that there are no vacancies in the lattices (see text). [b] Standard coordinates would be 0.336 25 (3), $x + ^1/_2$, $^1/_4$.

photographs, and only two of them showed relatively few extra reflections in addition to those expected for the tetragonal phase. A reasonable set of cell parameters from lists of randomly registered reflections on the diffractometer was obtained only from the stronger reflections. This suggested that there might be severe interference from the satellite crystals, so an initial orientation matrix was determined by using only reflections fitting a tetragonal cell, which also indicated that the cell was body-centered. No reflection conditions were imposed during the data collection. Three ψ-scans were employed for absorption correction.

The data set confirmed the centering, and it also contained weak but statistically significant reflections in 30 out of 80 instances where systematic absences normally occur for a W_5Si_3-type structure ($I4/mcm$), namely, for $h0l$ (or $0kl$) with h (k) and $l = 2n + 1$. Since over 90% of the other measured reflections were observed, the result was taken to mean that there must be a real reduction in symmetry in the structure. The only subgroup in the same Laue class with the observed absence conditions, $I422$ (no. 97), was subsequently found to be correct. Satisfactory solutions could not be found in other plausible space groups that lacked the subgroup relationship.

The initial model was again found with SHELXS-86. The refinement went well to $R = 2.2\%$, $R_w = 5.2\%$ with anisotropic thermal parameters and a secondary extinction correction. A partial substitution of Fe by Sn in the two independent antiprism centers present with this space group was suggested by their large effective scattering. The amounts of tin substitution were roughly estimated from the iron multiplicities and so refined, after which the thermal parameters behaved normally and both could be refined simultaneously. However, R_w (3.6%) and goodness of fit (1.89) were still somewhat high, and there were 11 reflections for which $\Delta F/\sigma_F > 5.0$. The worst was for (110), for which $\Delta F/\sigma_F = 22.4$. This was taken to arise from an accidental interference from a satellite crystal, and so the reflection was discarded. This changed the refined structure very slightly, but the statistics improved significantly: $R = 1.7\%$, $R_w = 2.2\%$, GOF = 1.16, and only one reflection now had $\Delta F/\sigma_F > 5$. The composition refined to $Zr_5Sn_{2.28(2)}Fe_{0.72(2)}$ when only Zr1 was held fixed; this compares reasonably well with the average EDX result for crystals in the initial button, $Zr_5Sn_{2.17}Fe_{0.77}$.

The correct enantiomer was confirmed by comparison of F_o and F_c values for 23 reflections for which the choice had the largest effect on F_c. The result was 15:8 in favor of that reported.

Because there are only subtle differences in the dimensions of the two centered antiprisms, based entirely on the z parameter of Zr2, a refinement with this parameter fixed at the ideal value ($z = ^3/_4$) was tried. This resulted in 0.1% greater R indexes, while parameters applying to the mixed Fe–Sn sites changed by 2σ or less. However, the average of F_o–F_c for the reflections that were violations in the ideal $I4/mcm$ was about 15% higher.

Another relevant observation was that the z parameter of Zr2 had a standard deviation about 10 times that of the other positional parameters. Coupling of the z parameter refinement with the multiplicities of Fe, Sn sites was not the cause. The implication is that the Zr2 atoms were slightly disordered along the c direction. Space group $I4$, a subgroup of $I422$ in the lower Laue class, was also explored to see whether the 2-fold axes perpendicular to $\vec{c}$ in the latter were responsible. In fact, standard deviations of all z parameters were now large, and the thermal parameters of Fe2, Sn3 became very anisotropic.

With these results, we concluded that the original refinement in the space group $I422$ was the correct one and that the behavior of the Zr2 atoms was probably a reflection of the random occupancies of the centers of the Zr2 antiprisms by Sn and Fe atoms of somewhat different sizes.

Zr_6Sn_2Fe. Some regular hexagonal plate crystals obtained after annealing an arc-melted button of the composition $Zr_6Sn_{1.8}Fe_{1.0}$ (see Results) were sealed in glass capillaries. Oscillation photographs showed most of these to be single. Random reflections located and tuned by the diffractometer gave an hexagonal unit cell, and two octants of reflection data collected on this basis indicated Laue symmetry $6/mmm$ with no systematic absences. Among the five possible space groups, $P\bar{6}2m$ was selected since the powder pattern had already been identified as that of a Zr_6Al_2Co-type material (above). The corresponding atom positions were used for the initial model. Refinement with isotropic thermal parameters yielded $R = 7\%$, $R_w = 9\%$. However, further refinement did not give much improvement in the residuals until a secondary extinction correction was applied, which gave convergence at $R = 2.6\%$, $R_w = 2.9\%$. The refined composition $Zr_3Zr_{2.99(2)}Sn_{1.98(1)}Fe_{1.00(1)}$ indicated the absence of substitutional defects, and so the atoms were returned to unit occupancy. The largest residual electron density, 1.9 e$^-$/Å^3, was close to Zr1. The other possible enantiomer gave residuals that were 0.6–0.8% higher.

The refined parameters and important bond lengths for the three structures studied are listed in Tables II and III. More crystal and refinement data, the anisotropic displacement parameters, and the structure factor data are available as supplementary material (see the paragraph at the end of the article).

Results and Discussion

Antimony Systems. Attempts to prepare the iron analogue of the stable Zr_5Sb_3Co, where interstitial cobalt is bound within an Mn_5Si_3-type structure,[2] regularly gave $ZrFe_2$ plus a phase with the Mn_5Si_3 structure and a composition near $Zr_5Sb_{3.3}Fe_{0.3}$ that presumably reflects a mixed Sb–Fe occupancy of the interstitial position. Reduction of the antimony content in an effort to obtain a simpler

Table III. Important Distances (Å) in $Zr_5Sb_{2.55}Fe_{0.45}$, $Zr_5Sn_{2.3}Fe_{0.7}$, and Zr_6Sn_2Fe

	$Zr_5Sb_{2.55}Fe_{0.45}$	$Zr_5Sn_{2.3}Fe_{0.7}$	$Zr_6Sn_2Fe^c$
Zr1–Zr1	2.7675 (7)	2.7397 (3)	
Zr2–Zr2	3.5866 (9)	3.5338 (7)	
Zr2–Zr2 (□–□)	3.2471 (9)	3.231 (4)	
		3.205 (4)[a]	
	3.5219 (9)	3.484 (4)	
		3.460 (4)[a]	
Zr2–Zr2 (interchain)	3.245 (1)	3.383 (1)	
Zr1–Zr2 (interchain)	3.5383 (6)	3.618 (1)	
		3.611 (1)	
Zr2–Sb1, Sn1, Fe	2.8891 (6)	2.853 (1)	
Zr2–Sn3, Fe2		2.846 (1)	
Zr1–Sb2, Sn2	2.9025 (6)	2.9282 (4)	
Zr2–Sb1, Sn1	2.9389 (7)[b]	2.9605 (6)[b]	
	2.9725 (6)[b]	3.0213 (5)[b]	
	3.2195 (8)	3.227 (2)	
		3.240 (2)	
Zr1–Sn			3.0094 (4)
Zr2–Sn			3.0678 (8)
Zr1–Zr1			4.2491 (8)
Zr1–Zr2			3.369 (1)
			3.2464 (8)[d]
Zr2–Zr2			3.384 (2)
Zr1–Fe			3.130 (1)
Zr2–Fe			2.6182 (9)

[a] Around the more nearly equally populated Fe2–Sn3 site. [b] Normal to *c*. [c] All atoms have a like-atom repeat at 3.4863 (5) Å ($\vec{c}$). [d] Within tricapped trigonal prism.

Table IV. Formation of the W_5Si_3-Type Phase in the Zr–Sb–Fe System

rxn	compsn[a] (Zr:Sb:Fe)	condns[b]	results[c]
1	5:2.47:0.5	AM	W
		AN	W[d]
2	5:2.55:0.67	AM	W + M (trace) + $ZrFe_2$ (trace)
		AN	W + M + $ZrFe_2$
3	5:2.53:0.67	AM	W + $ZrFe_2$
4	5:2.51:0.62	AM	W + $ZrFe_2$ (trace)
		AN	W + M (trace) + $ZrFe_2$
5	5:2.5:0.33	AM	W + Y
		AN	W + Y
6	5:2.67:0.5	AM	W + M
		AN	W + M
7	5:2:0.42	AM	W + Z[e] + β-Zr(Sb)

[a] Loaded compositions; the analytical composition for some of the samples are given in the text. [b] AM, arc-melting; AN, annealing of the previous arc-melted sample at 1200 °C for 3 days. [c] Phases were identified by both EDX measurements and powder patterns. W, W_5Si_3-type; M, Mn_5Si_3-type with a composition near $Zr_5Sb_{3.3}Fe_{0.3}$ (lower limit); Y, Y_5Bi_3-type; Z, Zr_6Al_2Co-type. [d] $Zr_5Sb_{2.58}Fe_{0.53}$ by SEM; a = 11.0885 (3), c = 5.5420 (3) Å. [e] a = 7.706 (1), c = 3.773 (1) Å.

product such as $Zr_5Sb_3Fe_x$ led instead to a tetragonal phase. EDX analyses and a single-crystal structural study showed this was $\sim Zr_5Sn_{2.5}Fe_{0.5}$ in a W_5Si_3-type structure with iron substituting for some antimony (below). This result led to the synthetic and analytical studies to determine the phase characteristics of the new material, Table IV. Reactions with the composition $Zr_5Sb_{2.5}Fe_{0.5}$ were found to yield a pure phase with W_5Si_3-structure both before and after an annealing treatment, and SEM-EDX analyses also showed that both samples consisted of homogeneous single phases. Some (0.1–0.2%) lattice parameter shrinkage was observed on annealing, but such effects are common[2,6,7] and presumably reflect improved ordering.

The next four reactions, Table IV, were designed to diagnose phase stability on variation of the iron content while the Zr:Sb ratio was held near 5:2.5. Increased iron led to the appearance of $ZrFe_2$ and, now that the sample

Table V. Products in $Zr_5Sb_{2.5}T_{0.5}$ Syntheses (T = Co, Ni, Ru, and Rh)[a]

	rxn condnts[b] (°C, days)	products Zr:Sb:T[c]	phase[d] (%)	a	c
Co	AM	5:2.55:0.37	W (80)	11.095 (2)	5.541 (1)
		6:2.34:0.69	Z (20)	7.741 (1)	3.686 (1)
	AN (1100, 30)	5:2.5:0.35	W	11.100 (1)	5.540 (1)
			Z (trace)		
Ni	AM	5:2.45:0.43	W (65)	11.100 (2)	5.527 (1)
		5:3.3:0.3	M (25)	8.463 (1)	5.772 (1)
		6:2.44:0.65	Z (10)	7.69 (1)	3.78 (1)
	AN (1200, 30)	5:2.55:0.4	W (85)	11.093 (2)	5.524 (1)
		6:2.35:0.7	Z (10)	7.689 (5)	3.792 (5)
			M (trace)		
Ru	AM		W (60)	11.089 (3)	5.575 (2)
			M (40)	8.468 (4)	5.818 (4)
Rh	AM	5:2.45:0.65	W (40)	11.091 (2)	5.549 (1)
		5:3.1:0.14	M (60)	8.479 (1)	5.787 (2)
	AN (1100, 30)	5:2.5:0.55	W (70)	11.107 (2)	5.563 (1)
		5:3.26:0.3	M (30)	8.592 (1)	5.855 (1)

[a] All reactions were loaded as $Zr_5Sb_{2.5}T_{0.5}$. [b] AM, arc-melting; AN, annealing of the previously arc-melted samples. [c] Compositions of corresponding phases as determined by EDX. [d] Abbreviations and cell types: W, W_5Si_3, tetragonal; M, Mn_5Si_3; Z, Zr_6Al_2Co, both hexagonal. Cell dimensions are in angstroms.

was antimony-richer than $Zr_5Sb_{2.5}Fe_{0.5}$, to a Mn_5Si_3-type phase near $\sim Zr_5Sb_{3.2}Fe_{0.2}$ in addition to the major phase, viz.

$$\text{"}11Zr_5Sb_{2.5}Fe_{0.67}\text{"} \rightarrow 10Zr_5Sb_{2.5}Fe_{0.5} + 0.8Zr_5Sb_{3.2}Fe_{0.2} + 1.1ZrFe_2$$

With a smaller amount of iron, a Y_5Bi_3-type phase also appeared, as observed before for binary antimony-limited compositions near Zr_5Sb_3.[13]

The last two reactions, Table IV, were run with varying amounts of antimony. An excess gives the Mn_5Si_3-type phase seen before, and a deficiency produces a hexagonal Zr_6Al_2Co-type phase (below) plus zirconium. EDX analyses of the most antimony-deficient sample gave $\sim Zr_6Sb_{2.3}Fe_{0.7}$ for the Zr_6Al_2Co-type portion and $\sim Zr_5Sb_{2.42}Fe_{0.53}$ for the W_5Si_3-type phase. We conclude that the W_5Si_3-type phase in this system has a narrow composition range at ~1200 °C, from $\sim Zr_5Sb_{2.40}Fe_{0.60}$ (reaction 3) with a = 11.083 (1), c = 5.540 (1) Å to $\sim Zr_5Sb_{2.55}Fe_{0.44}$ (reaction 6) with a = 11.107 (1), c = 5.554 (1) Å. The sums of the antimony and iron contents were always close to 0.60 per zirconium, implying that there are no vacancies in the structure.

On the basis of these observations, analogous phases were studied in which other transition-metal atoms (T) substitute for iron in $Zr_5Sb_{2.5}T_{0.5}$ phases, Table V. All the iron group elements and their fifth-period congeners Ru and Rh form the W_5Si_3 phase with almost the same feature, that is, with a composition near $Zr_5Sb_{2.5}T_{0.5}$ apparently necessary for stability. The phase compositions determined by EDX methods varied modestly on annealing, mainly for the Mn_5Si_3-type examples, and these implied mixed Sb–T populations in both the Mn_5Si_3 interstitial site and in the cobalt site in Zr_6Al_2Co-type examples as well. The Mn_5Si_3 examples appear only with higher antimony concentrations.

A tetragonal W_5Si_3-type structure with a composition $Zr_5Sb_{2.55(1)}Fe_{0.45(1)}$ was refined from single-crystal X-ray data. All of the Sb–Fe mixing occurs on the main-group element (Sb1) site that ideally centers square antiprisms of zirconium. The X-ray analysis assumed there were no vacancies at this point, in accord with the SEM-EDX

(13) Garcia, E.; Corbett, J. D. *Inorg. Chem.* **1988**, *27*, 2353.

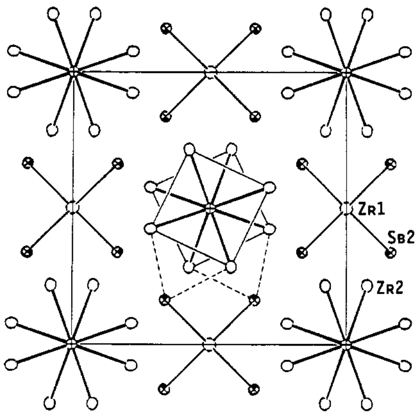

Figure 1. Projection of the tetragonal structure of $Zr_5Sb_{2.55}Fe_{0.45}$ down the short *c* axis. The Zr2 (○) antiprism about the $Sb_{0.55}Fe_{0.45}$ site (⊕) in the center of the cell and the tetrahedra of Sb2 (⊕) about Zr1 are emphasized. Other short Zr2–Zr2 and Zr1–Zr2 separations are not shown (see text). Dashed lines illustrate the commonality of antimony to both chains (97% probability ellipsoids).

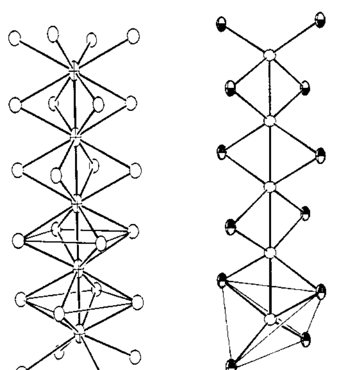

Figure 2. Side view illustrating the geometric essence of the chains of $(Sb,Fe)Zr_{8/2}$ (left) and $Sb_{4/2}Zr$ (right) in $Zr_5Sb_{2.55}Fe_{0.45}$. One antiprism and one tetrahedron are lightly outlined (97%).

results. A convenient geometric description of the structure starts with square antiprisms (Zr2) that share opposite square faces to generate infinite chains $^1_\infty[Zr_{8/2}(Sb_xFe_{1-x})Sb_{8/2}]$. One of these is highlighted in Figure 1 in a projection down the short *c* axis. The twist angle between the squares is actually 39.1° rather than the ideal 45°. The structure also contains parallel, linear chains of zirconium with a very short repeat (2.77 Å = $c/2$) that lie within edge-shared $^1_\infty[ZrSb_{4/2}]$ tetrahedra centered on the side faces of the cell in this view. The two chains are not as independent as this description suggests, however; the same antimony atoms envelope both chains, those in the tetrahedra also bridging pairs of edges of the zirconium antiprisms (Figure 1, dashed lines). Side views of the two chains are shown in Figure 2 with these interconnections omitted. Other short Zr–Zr separations in this material will be noted later in a comparison of structures.

Tin in W_5Si_3-Like Phases. Tin analogues of the foregoing antimony phases are closely related but with some contrasts; only iron seems to form a W_5Si_3-like phase, this has a higher iron content, and a lower crystal symmetry yields two different populations for the antiprismatic chain-centering Sn–Fe atoms. As-cast samples are invariably composed of Mn_5Si_3-type phases and $ZrFe_2$, Table VI, and only after annealing do W_5Si_3-type phases appear. The optical yields of the W_5Si_3 example, 80–90%, were achieved for compositions $Zn_5Sn_{2+x}Fe_{1-x}$, $0 < x < 0.28$, judging from the intensity distributions in the powder patterns (Table VI) and the X-ray analysis. This range

Table VI. Formation of W_5Si_3-Type Phases in Zr–Sn–T Systems, T = Fe, Co

rxn	compsn[a] (Zr:Sn:T)	condns[b] (°C, days)	results[c]
Fe	5:2.5:0.5	AM	M + $ZrFe_2$
		AN (1000, 7)	W + M
	5:2.25:0.75	AM	M + $ZrFe_2$
		AN (1050, 7)	W (a = 11.1663 (9), c = 5.4747 (8)) + M (trace) + $ZrFe_2$ (trace)
	5:2.0:1.0	AM	M + $ZrFe_2$
		AN (1000, 7)	W (a = 11.160 (1), c = 5.4719 (8)) + Z (trace) + $ZrFe_2$ (trace)
	5:2.0:1.0	AM, AN (1350, 8)	W ($Zr_5Sn_{2.18}Fe_{0.77}$;[d] a = 11.1763 (7), c = 5.4794 (6)) + $ZrFe_2$ (≤2%)
Co	5:2.0:1.0	AM	M + impurity
		AN (1000, 10)	Z (40%) + M (60%)

[a] Loaded composition. [b] AM, arc-melting; AN, annealing of the previously arc-melted sample. [c] W, W_5Si_3-type; M, Mn_5Si_3-type; Y, Y_5Bi_3-type; Z, Zr_6Al_2Co-type. Trace is <5%. Dimensions are in angstroms. [d] Average EDX result.

was also supported by (unconstrained) EDX results of $\sim Zr_5Sn_{1.95}Fe_{1.05}$ and $\sim Zr_5Sn_{2.25}Fe_{0.75}$ for this portion of annealed compositions $Zr_6Sn_{1.8}Fe_{1.2}$ and Zr_6Sn_2Fe (both primarily Zr_6Al_2Co-type products, below). Analogous reactions with cobalt gave only Zr_6Al_2Co- and Mn_5Si_3-type phases upon annealing.

The refined W_5Si_3-like structure for this sample is iron-richer than found with antimony, $Zr_5Sn_{2.28(2)}Fe_{0.72(2)}$ and near the inferred lower limit for iron (above). The acentric space group $I422$ lacks all mirror planes present in the parent W_5Si_3 ($I\bar{4}/mcm$, Figure 1) although the two independent, centered Fe–Sn sites in adjacent antiprisms retain 42 symmetry. The shared faces of the antiprisms are still the same size, but these are no longer equally spaced, although their alternate displacements in $\vec{c}$ are only 0.020 Å. More importantly, the two mixed Sn–Fe populations refine to distinctly different values, 91 (2)% and 52 (2)% iron (assuming no vacancies). Surprisingly, the latter occurs in the slightly smaller antiprism although the refined Zr–Sn,Fe distances differ by only 0.007 Å (5σ). The violations of the systematic absences for an ideal W_5Si_3 arrangement come solely from the unfixed z coordinate of Zr2 and the unequal atomic distributions of the mixed Sn and Fe. The latter appear to contribute significantly more to the observations than the deviation of z from $^3/_4$, which may be an artifact of the refinement.

There appears to be no precedent for a W_5Si_3-like structure with this lower symmetry, possibly because it generally cannot be distinguished from a W_5Si_3-type by powder pattern means. The strongest additional line calculated for the Guinier pattern is only 0.4% of I_{max}.

Previously reported analogues of both structures involve only mixed main-group elements, e.g., Co_5Si_2B, Fe_5Si_2B,[14] Ni_5Si_2B,[15] and Nb_5Sn_2Si,[16] although the binary β-Ti_3Sb also exhibits the same diposition, Ti_5Sb_2Ti.[17] The second and third actually exhibit a Fe or Ni deficiency within the tetrahedral chains, e.g., $Fe_4Fe_{0.86}Si_2B$. All have been studied by powder or single-crystal film methods.

Some rationale for the formation of the W_5Si_3-like phase on substitution of iron in Zr_5Sb_3 or Zr_5Sn_3 can be obtained from Pettifor's structure maps.[18,19] Pettifor assigned

(14) Aronsson, B.; Lundgren, G. *Acta Chem. Scand.* **1959**, *13*, 433.
(15) Uraz, A. A.; Rundqvist, S. *Acta Chem. Scand.* **1970**, *24*, 1843.
(16) Horyn, R.; Lukaszewicz, K. *Bull. Acad. Polon. Sci., Ser. Sci. Chim.* **1970**, *18*, 59.
(17) Kjekshus, A.; Gronvold, F.; Thorbjornsen, J. *Acta Chem. Scand.* **1962**, *16*, 1493.

Table VII. Characteristics of Zr_6Al_2Co-Type Phases in Zr–Sn–T Systems, T = Fe, Co

T	compsn[a] (Zr:Sn:T)	condns[b] (°C, days)	results[c]
Fe	6:1.8:1.2	AM	M + $ZrFe_2$ (10%) + impurity (10%)
		AN (1000, 8)	Z + $ZrFe_2$ (5%) + W (10%) + M (2%)
Fe	6:2.0:1.0	AM	M + $ZrFe_2$ (10%) + impurity (10%)
		AN (1000, 7)	Z + W (15%)
Fe	6:1.8:1.0	AM, AN (1050, 7)	Z + W (<5%); very brittle
Co	6:2.0:1.0	AM, AN (1000, 10)	Z (a = 7.9450 (8), c = 3.4993 (7) Å) + M (15%) + β-Zr (<3%)
		GRST (1000, 9)	Z (a = 7.9386 (6), c = 3.5102 (7) Å) + M (15%)

[a] Loaded composition. [b] AM, arc-melting; AN, annealing of the previously arc-melted sample; GRST, previous sample was ground, pelleted, and sintered. [c] W, W_5Si_3-type; M, Mn_5Si_3-type; Z, Zr_6Al_2Co-type.

Mendeleev numbers[20] in such a way that elements in one group have successive numbers, and he then defined structural fields on this basis. In the A_5B_3 binary map, the point corresponding to Zr_5Sb_3 falls in the Mn_5Si_3-type region, as it should, but the substitution of iron or any other of the transition elements tried in this study for antimony would move the point toward the W_5Si_3 region. Since no boundary between these two structure types was established in the map, it is not clear what amount of substitution is needed to form a W_5Si_3-type structure. The same expectation holds for Zr_5Sn_3, which also forms in Mn_5Si_3-type structure. However, why a cobalt example does not always form cannot be answered with this map. Of course, the stability of $ZrFe_2$ also plays an important role in determining the composition of the W_5Si_3-type products.

Zr_6Al_2Co-Type Phases. A new phase was seen in compositions near Zr_5Sn_2Fe, and its powder pattern was found to be in good agreement with that for a Zr_6Al_2Co-type phase. Several compositions around this were studied in an effort to clarify the system, Table VII. As-cast samples contained only a Mn_5Si_3-type phase and $ZrFe_2$, but annealing at 1000 °C for 7 days was sufficient to produce the pattern of what was presumed to be the peritectically decomposing tin–iron analogue ~Zr_6Sn_2Fe. However, not a single sample prepared in this way was single phase. Even reactions with the stoichiometry determined by the single-crystal structural analysis (below) showed ~15% of a W_5Si_3-type phase (and possible $ZrFe_2$) in the powder pattern. Incomplete equilibration is evident, perhaps because of a gross composition inhomogeneity produced by the arc-melting.[6] Nonetheless, the very brittle, annealed $Zr_6Sn_{1.8}Fe_{1.0}$ product yielded single crystals, and the structure was refined as the expected Zr_6Al_2Co-type. The lattice parameters of this phase do not change with loaded composition. This and the stoichiometric result of the structure refinement, $Zr_6Sn_{1.99(1)}Fe_{1.00(1)}$, indicate a line phase without vacancies near 1050 °C.

The analogous cobalt compound also forms; however, no further attempts were made to elucidate the composition width or the details of the structure. Zr_6Al_2Co-type phases are also formed with antimony instead of tin, namely, as a minor component in as-cast samples of the composition $Zr_5Sb_{2.5}T_{0.5}$ with T = Fe, Co, Ni, Ru (Tables IV and V). Antimony evidently again substitutes for some

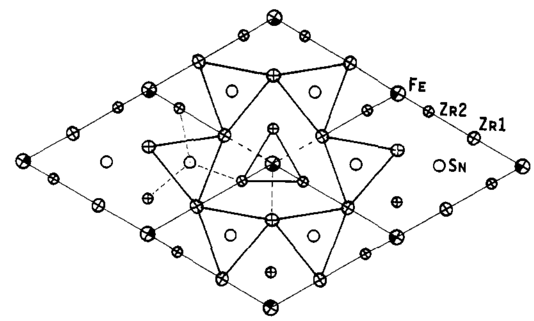

Figure 3. Projection of the hexagonal structure of Zr_6Sn_2Fe along the short (3.49 Å) c axis. A portion of the zirconium (⊕) trigonal prisms centered by tin (○) or iron (⊕) are emphasized. The two types of prisms differ in elevation by c/2. One set of the prism face-capping interconnections between different kinds of trigonal prisms is shown dashed (99.5% ellipsoids).

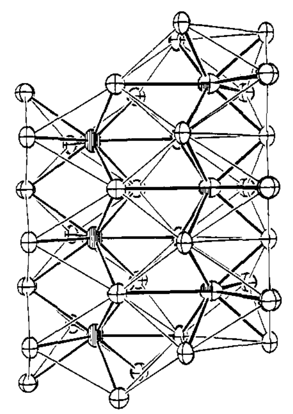

Figure 4. Side view of the pair of interconnected trigonal prismatic chains shown in Figure 3. The tin-centered chain is on the left and the iron-based portion is on the right with the nine Zr–Fe interactions given heavier emphasis. Iron is partially and tin is wholly shaded (99.5%).

of the T element since the compositions determined by EDX analyses corresponded to a general formula near $Zr_6Sb_{2.3}T_{0.7}$.

The structure of Zr_6Sn_2Fe is shown in Figures 3 and 4 in views along and normal to the hexagonal c axis, respectively. The result can be assembled starting with trigonal prism $(Zr2)_6Fe$ at the origin together with a larger pair of $(Zr1)_6Sn$ trigonal prisms centered on $^1/_3$, $^2/_3$, $^1/_2$, etc. (Figure 3). The tin-centered prisms also share all edges parallel to $\vec{c}$ to generate a network in the ab plane. Each type of prismatic unit also shares opposite triangular faces with like units to generate confacial chains parallel to $\vec{c}$, viz., $[(Zr2)_{6/2}Fe][(Zr1)_{6/4}Sn)]_2$, Figure 4. Finally, such a high concentration of centered (Fe, Sn) atoms relative to zirconium leads to a secondary condensation between the two types of prismatic units such that zirconium atoms in each prism also cap rectangular faces in the other. These interactions, shown with dashed lines in Figure 3, lead to a classic tricapped trigonal prismatic environment for both Sn and Fe. The Fe–Zr distances in the $FeZr_6$ prisms seem particularly short, 2.619 (1) Å, relative to 2.853 (1) Å for the 91% Fe site in $Zr_5Sn_{2.3}Fe_{0.7}$ (above). However, similar results are found for iron within bicapped trigonal prisms in Zr_3Fe, where d(Zr–Fe) is 2.63 and 3.03 Å to prismatic and capping zirconium, respectively.[21] On the other hand, roughly octahedral Zr_6Fe units in the more oxidized $Cs_{0.6}Zr_6I_{14}Fe$ have $\bar{d}$(Zr–Fe) as short as 2.48 Å,[22] suggesting

(18) Pettifor, D. G. *J. Phys. C: Solid State Phys.* **1986**, *19*, 283.
(19) Pettifor, D. G. *Mater. Sci. Technol.* **1988**, *4*, 675.
(20) Pettifor, D. G. *New Scientist* **1986**, *May 29*, p 48.
(21) Buschow, K. H. J. *J. Less-Common Met.* **1981**, *79*, 243.
(22) Hughbanks, T.; Rosenthal, G.; Corbett, J. D. *J. Am. Chem. Soc.* **1988**, *110*, 1511.

there is a good deal more in electronic effects in these compounds than meets the eye!

Except for Zr_6Al_2Co analogues with T = Fe, Ni,[9] there are only a couple of other examples of this structure type, Ni_6Si_2B[23] and (anti-) β-K_2UF_6.[24,25] The newly identified Zr_6Sn_2Fe has been found by powder pattern comparison to be identical with the θ-phase reported by Tanner and Levinson[26] in a study of a portion of the Zr–Sn–Fe system. They judged this to be a line phase with a composition near $Zr_6Sn_{1.7}Fe_{1.2}$. The same phase has also been identified by powder X-ray methods as a precipitate after irradiation of β-Zircaloy-4 with nitrogen ions.[27,28]

There is nothing particularly notable about any other of the Zr–Sb, –Sn, –Fe distances in the structures reported here relative to those in several Mn_5Si_3-type examples that have recently been studied for the same or similar elements.[2,4,6,13,29] On the other hand, Zr–Zr bonding and some geometric aspects among these three types do provide some interesting variations and comparisons.

General Comparisons. It is not clear why the foregoing W_5Si_3-like phases need two such chemically distinct elements centered in the anti-prisms and in almost fixed ratio in each instance in order to stabilize these, but the effect is presumably electronic. Among binary zirconium compounds, the W_5Si_3 structure is known only for Zr_5Al_3, while this arrangement is distinctly more common with the electron-poorer rare-earth elements or with Ti, Nb, and Ta when either group is combined with Ga or, for the former, In and Tl.[10] Involvement of silicon, germanium, or tin as the main-group element (Ma) evidently again provides W_5Si_3-type phases only with earlier or later transition elements, namely, from group 5 or 6 with Si or Ge or for La, Ce, Pr with Sn.[10] The sparsity of Zr_5Ma_3 examples with the W_5Si_3 structure must arise because of the greater stability of the Mn_5Si_3-type compounds formed between Zr (Hf, Ti) and many of these main-group elements, either as binary phases or in ternaries Zr_5Ma_3Z with interstitial Z. Zr_5Al_3 also exists as a binary phase with this structure.[30] The conversion to a W_5Si_3-like product $Zr_5Ma_{3-x}T_x$ with Ma = Sb, Sn, $x \sim 0.5$, and T = Fe, Co, etc., thus appear to be quite specific.

The most interesting structural comparison is between the Mn_5Si_3- and W_5Si_3-types. The former contain parallel confacial $Mn_{6/2}Si_{6/2}$ trigonal antiprismatic chains and, again, linear manganese chains. These share the same Si atoms which give the second type of manganese a twisted antiprismatic environment. Interchain interactions are relatively long, 3.49–3.54 Å in the known binaries Zr_5Sb_3[13] and Zr_5Sn_3[6] but still somewhat shorter than Zr–Zr separations within the "octahedral" chains; however, extended Hückel MO calculations on Zr_5Sb_3 indicate the interchain "bonds" have relatively low overlap populations.[2] The linear chains in these two phases are evidently strongly bonded, with repeat distances around 2.90 Å [d_1(Zr) = 2.918 Å]. The alternative W_5Si_3 structure appears to form in generally electron-richer systems, e.g., Nb_5Ga_3, Nb_5Ge_3, and Mo_5Ge_3 either alone or with a Mn_5Si_3 form as well.[10] (Exceptions include Zr_5Al_3 (dimorphic) and a number of rare-earth-metal examples such as La_5Sn_3.) The electronic factors involved in the structural differentiation are unknown and worthy of study.

The most interesting feature of the Mn_5Si_3-type phases formed by zirconium (and rare-earth metals) is their avidity to bond interstitially a wide variety of a third element Z, generally those elements to the right of Fe in the periodic table. These occur in the center of every metal octahedron, obviously gaining strong Zr–Z interactions with small loss of Zr–Zr bonding.[2-4] The alternative with iron (and some neighboring elements T) is to form the zirconium-richer $Zr_5Ma_2(Ma_xT_{1-x})$ described here, where the added elements is an integral part of the W_5Si_3 structure, that is, centered in the antiprismatic chain. The change from a Mn_5Si_3- to a W_5Si_3-type phase is accompanied by not only an increase in coordination number of the centered (T, Z) element from six to eight but also significantly closer Zr–Zr separations, namely, 3.20–3.24 and 3.24–3.38 Å within and between the square anti-prismatic chains, respectively, and 2.74–2.77 Å along the linear chains in the compounds described here. A countervailing factor is the decrease in the number of zirconium near neighbors about Sb or Sn from five to four, largely in the environment of the linear zirconium string.

The next step to Zr_6Sn_2Fe represents an obviously efficient way of achieving efficient bonding with nine-coordinate tin and iron. This as well as the substituted W_5Si_3-type phases appears to have considerably narrower electronic requirements than do the wide variety of compounds with a Mn_5Si_3(Z)-type structure.

Acknowledgment. We are indebted to H. F. Franzen for the use of the arc-melting and induction-heating equipment, to A. Guloy for assistance with the high-temperature vacuum furnace, and to R. A. Jacobson for the diffractometer facilities. Personnel at the Analytical Electron Microscopy Laboratory, ERI, were very accommodating.

Registry No. $Zr_5Sb_{2.5}Fe_{0.5}$, 129124-24-9; $Zr_5Sb_{3.3}Fe_{0.3}$, 129124-25-0; $Zr_5Sb_{3.2}Fe_{0.2}$, 129124-26-1; $Zr_6Sb_{2.3}Fe_{0.7}$, 129124-27-2; $Zr_5Sb_{2.42}Fe_{0.53}$, 129124-28-3; $Zr_5Sb_{2.4-2.55}Fe_{0.44-0.6}$, 129124-29-4; $Zr_5Sb_2Fe_{0.42}$, 129124-30-7; $ZrFe_2$, 12023-45-9; $Zr_6Sn_{1.99}Fe_{1.0}$, 129124-31-8; $Zr_5Sb_{2.5}Co_{0.5}$, 129124-32-9; $Zr_6Sb_{2.34}Co_{0.69}$, 129124-33-0; $Zr_5Sb_{2,5}Ni_{0,5}$, 129124-35-2; $Zr_6Sb_{2.3}Ni_{0.7}$, 129124-36-3; $Zr_5Sb_{2.5}Rh_{0.5}$, 129124-40-9; $Zr_5Sb_{2.5}Ru_{0.5}$, 129124-41-0; $Zr_6Sb_{2.3}Ru_{0.7}$, 129124-42-1; $Zr_5Sn_{1.95}Fe_{1.05}$, 129124-44-3; $Zr_5Sn_{2.25}Fe_{0.75}$, 129124-45-4; $Zr_5Sn_{2.8}Fe_{0.72}$, 129124-46-5; $Zr_6Sn_{1.8}Fe_{1.0}$, 129124-47-6; $Zr_5Sb_{2.55}Fe_{0.45}$, 129124-48-7; $Zr_5Sn_{2.3}Fe_{0.7}$, 129124-49-8; Zr_6Sn_2Fe, 129124-50-1; Zr_5Rh_2, 129124-51-2; Zr_5Ru_2, 129124-52-3; Zr, 7440-67-7; Sb, 7440-36-0; Sn, 7440-31-5; Fe, 7439-89-6; Co, 7440-48-4; Ni, 7440-02-0; Rh, 7440-16-6; Ru, 7440-18-8.

Supplementary Material Available: Tables of crystallographic data and anisotropic displacement parameters (2 pages); tables of observed and calculated structure factors for $Zr_5Sb_{2.5}Fe_{0.5}$, $Zr_5Sn_{2.3}Fe_{0.7}$, and Zr_6Sn_2Fe (8 pages). Ordering information is given on any current masthead page.

(23) Rundqvist, S.; Jellinek, F. *Acta Chem. Scand.* **1959**, *13*, 425.
(24) Zachariasen, W. H. *Acta Crystallogr.* **1948**, *1*, 265.
(25) Wells, A. F. *Structural Inorganic Chemistry*, 5th ed.; Clarendon Press: Oxford, 1984; p 1262.
(26) Tanner, L. E.; Levinson, D. W. *Trans. Am. Soc. Met.* **1960**, *52*, 1115.
(27) Yang, T. Y.; Yu, G. P.; Chen, L. J. *J. Nucl. Mater.* **1987**, *150*, 67.
(28) The reported[26] composition of the θ phase was incorrectly quoted in ref 27 in terms of weight fractions of the components.
(29) Garcia, E.; Corbett, J. D. *J. Solid State Chem.* **1988**, *73*, 452.
(30) Kim, S.-J.; Kematick, R. J.; Yi, S. S.; Franzen, H. F. *J. Less-Common Met.* **1988**, *137*, 55.